

Superlensing microscope objective lens

BING YAN,¹ ZENGBO WANG,^{1,*} ALAN L. PARKER,² YU-KUN LAI,³ P. JOHN THOMAS,⁴ LIYANG YUE,¹
AND JAMES N. MONKS¹

¹School of Electronic Engineering, Bangor University, LL57 1UT Bangor, UK

²Division of Cancer and Genetics, Cardiff University School of Medicine, CF14 4XN Cardiff, UK

³School of Computer Science and Informatics, Cardiff University, CF24 3AA Cardiff, UK

⁴School of Chemistry, Bangor University, LL57 2UW Bangor, UK

*Corresponding author: z.wang@bangor.ac.uk

Received 23 November 2016; revised 10 March 2017; accepted 13 March 2017; posted 13 March 2017 (Doc. ID 281397);
published 7 April 2017

Conventional microscope objective lenses are diffraction limited; they cannot resolve subdiffraction features of a size smaller than 250–300 nm under white lighting condition. New innovations are required to overcome this limitation. In this paper, we propose and demonstrate a new superlensing objective lens that possesses a resolution of 100 nm, which is a two-times resolution improvement over conventional objectives. This is accomplished by integrating a conventional microscope objective lens with a superlensing microsphere lens using a customized lens adaptor. The new objective lens was successfully demonstrated for label-free super-resolution imaging of 100 nm features in engineering and biological samples, including a Blu-ray disk sample and adenoviruses. Our work opens a new door to develop a generic optical superlens, which may transform the field of optical microscopy and imaging. © 2017 Optical Society of America

OCIS codes: (100.6640) Superresolution; (180.4243) Near-field microscopy; (180.5810) Scanning microscopy; (170.3880) Medical and biological imaging.

<https://doi.org/10.1364/AO.56.003142>

1. INTRODUCTION

An objective lens is the core element of an optical microscope, whose resolution is limited by the classical diffraction law as first formulated by the German physicist Ernst Abbe in 1873: the minimum distance, d , between two structural elements to be imaged as two objects instead of one is given by $d = \lambda/(2NA)$, where λ is the wavelength of light and NA is the numerical aperture of the objective lens [1]. The physical root stems from the loss of exponentially decaying evanescent waves in the far field that carry the high spatial frequency subwavelength information of an object [2].

The development of near-field scanning optical microscope (NSOM) opens the door to super-resolution research. It uses a tiny tip positioned close to an object's surface to collect evanescent waves in the near field [3]. Scanning the sample generates a super-resolution image whose resolution is determined by tip size instead of wavelength. Since the late 1990s, owing to the rise of metamaterials, nanophotonics, and plasmonics, the field of super-resolution research has grown extremely rapidly. A variety of super-resolution techniques were developed, including, for example, the Pendry–Veselago superlens [2,4], the optical superoscillatory lens [5], time-reversal imaging [6], the Maxwell fisheye [7], the scattering lens [8], and, most famously, super-resolution fluorescence microscopy techniques

[9–11], which won the 2014 Nobel Prize. However, none of these techniques would operate under white lighting sources, e.g., the conventional Halogen lamps or recent white LEDs, whose radiation covers a broadband electromagnetic spectrum. Monochromatic lasers are required. The solution to white light super-resolution appeared in 2011, when we first reported that a microsphere can work as a superlens under white lights and achieve a resolution between 50 and 100 nm [12–14]. The super-resolution arises from the microsphere's ability to focus light beyond the diffraction limit, a phenomenon known as “photonic nanojet” [15,16], and near-field collection of evanescent waves by the microspheres when in contact with imaged objects. This technique is label-free and has been further advanced by a number of groups across the world, including, for example, the development of confocal microsphere nanoscopy [14,17], solid immersion microsphere nanoscopy [18,19], microfiber nanoscopy [20], subsurface nano-imaging [21,22], and new microsphere superlens designs [23,24]. Very recently, we demonstrated a new superlens made from high-index nanobeads [25] and created what we believe is the world's first biological superlens using spider silks [26]. For better understanding of the field, please refer to our recent review article [14].

The imaging window of a microsphere lens is often very small, typically only a few micrometers. This requires a scanning

operation of the microsphere superlens to generate a complete image of a sample. There are a few demonstrations in the literature. Krivitsky *et al.* attached a fine glass micropipette to the microsphere lens to scan the particle [27]. Li *et al.* designed a “swimming lens” technique in which the microsphere lens was propelled and scanned across the sample surface by chemical reaction force in a liquid [28]. We proposed a coverslip superlens by encapsulating high-index microspheres (BaTiO_3 or TiO_2) inside a transparent host material (such as PMMA and PDMS) [29]. The microsphere was completely immersed inside the encapsulation material with its bottom touching the coverslip surface [see Fig. 1(a) side view]. This concept was also explored extensively by Darafsheh and Astratov *et al.* in the U.S. [18,30,31]. The coverslip superlens can be manually manipulated in a way similar to a classical coverslip, offering the freedom to position the particle lens at a desired location. Scanning of a microsphere superlens, however, requires synchronization with the microscope objective for full super-resolution image construction. This is difficult to achieve with the existing coverslip superlens design, which is separated from the objective lens. In this paper, we propose an improved design that solves the synchronization problem between the coverslip superlens and the objective lens. The idea is simple yet effective, using a custom-made lens adaptor to integrate these two lenses to form a superlensing microscope objective lens.

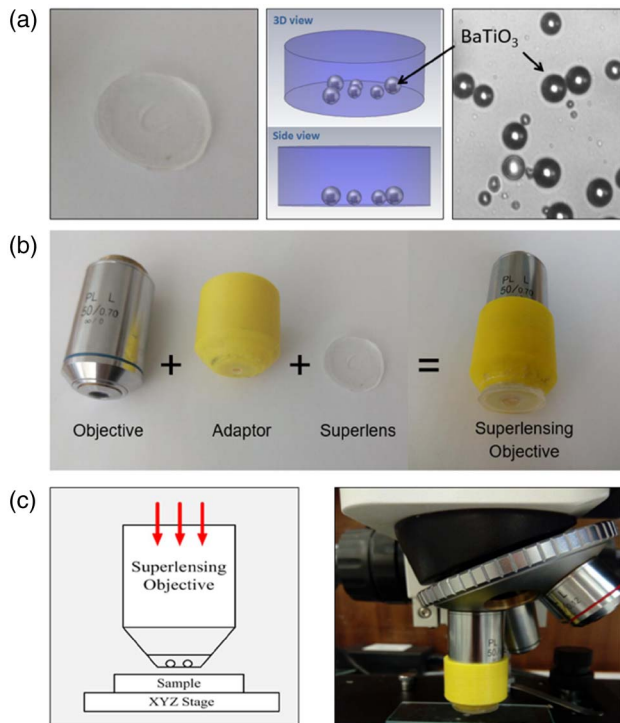


Fig. 1. Superlensing objective lens. (a) BaTiO_3 superlens was fabricated by encapsulating a monolayer of BaTiO_3 microsphere (3–80 μm diameter) inside a PDMS material. (b) Super objective was made by integrating a conventional microscope objective lens (e.g., 50 \times , NA: 0.70, or 100 \times , NA: 0.95) with a BaTiO_3 microsphere superlens using a 3D printed adaptor (c) Experimental configuration for super-resolution imaging using a developed objective that was fitted onto a standard white light optical microscope.

2. SUPERLENSING MICROSCOPE OBJECTIVE

The key concept and design of a superlensing microscope objective is illustrated in Figs. 1(b) and 1(c). A conventional microscope objective (OB) lens with a magnification factor between 40 \times and 100 \times , and a NA between 0.7 and 0.95 was selected. A lens adaptor was designed in CAD software (e.g., SolidWorks) and then printed with a Prusa 15 3D plastic printer. The adaptor has a tube size fit to the objective lens tube, with reasonable friction allowing up-down adjustment. A coverslip superlens [Fig. 1(a)] was bonded to the bottom end of the adaptor using high-adhesive glue. This results in an integrated objective lens consisting of conventional OB and a coverslip microsphere superlens (CMS). The imaging resolution will be determined by the coverslip superlens, while the conventional objective lens provides the necessary condition for illumination. The obtained superlensing lens can be easily fitted to any existing conventional microscopes. In this study, we used two brands of optical microscopes to prove the flexibility of the lens (Olympus BX60 and a low-cost ICM100 microscope) in usage.

The scanning was performed using a high-resolution nano-stage (P-611.3 NanoCube, Physik Instrumente), with a 1 nm resolution in the XYZ direction, and a travel range of 100 μm . Samples (Blu-ray disk, semiconductor chip, and a virus on a glass slider) were firmly bonded to the nano-stage using high-strength, double-sided sticking tape. In our experiments, the superlensing objective lens was kept static and the underlying nano-stage moved and scanned the samples across the objective lens. The imaging process was video recorded using a high-resolution camera (ToupCAM UCMOS 14000KPA, ToupTek Photonics). The video was then analyzed and frames were used to generate a stitched image of the sample. The focusing properties of the developed superlens were analyzed using classical Mie theory.

3. EXPERIMENTS

A. Static Imaging

The superlensing objective lens was carefully adjusted to maximum imaging contrast and image quality. The main adjustments were: (1) the lens adaptor was adjusted so that the top objective lens will pick up the virtual image generated by the bottom coverslip microsphere superlens; and (2) the light illumination angle was adjusted. An angle roughly between 10 and 40 deg will produce an enhancement in image quality, because the magnification factor is increasing with incident angles and there is a compromise between image quality and magnification factor [26]. Best imaging resolution is obtained in contacting mode where lens and samples contact each other. The resolution was found to be decreasing rapidly when the lens moved away from the sample surface. At about the wavelength distance (~ 600 nm) away, the super-resolution was completely lost (due to loss of evanescent wave contribution), which indicates the near-field nature of the technique. This inversely poses a technical challenge in scanning imaging as will be discussed below.

In the contacting mode, we carried out super-resolution imaging of several different samples, including a Blu-ray disk with 100 nm/200 nm features and adenoviruses (replication deficient

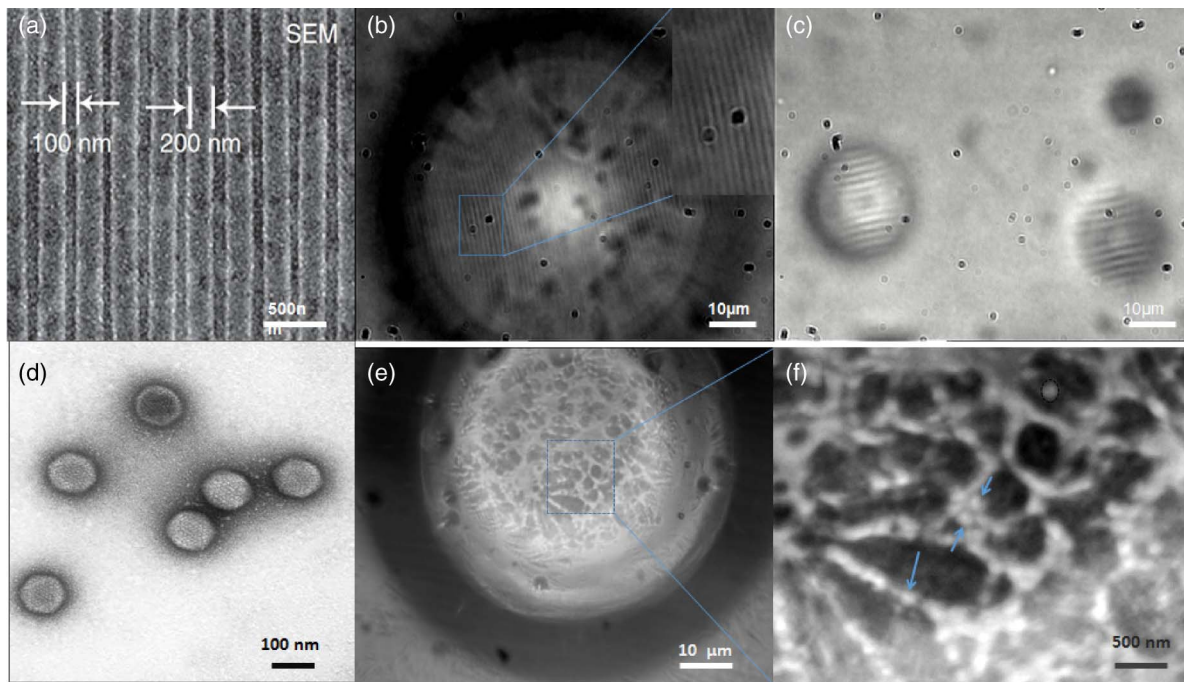


Fig. 2. Static super-resolution imaging of a Blu-ray and a virus by superlensing objective lens. (a) SEM image of a Blu-ray disk. (b) $67\ \mu\text{m}$ BaTiO_3 superlens imaging. (c) $18\ \mu\text{m}$ BaTiO_3 superlens imaging. (d) SEM of adenovirus. (e) $70\ \mu\text{m}$ BaTiO_3 superlens imaging of virus cluster. (f) Enlarged view of section of (e).

human adenovirus serotype 5 vector) with a size about $90\text{--}100\ \text{nm}$. Note that the superlensing objective lens in these tests could be slightly different from each other, to demonstrate the ability to achieve super-resolution with different lens configurations. As previously mentioned, the overall resolution is determined by the CMS, which consists of a BaTiO_3 microsphere ($3\text{--}80\ \mu\text{m}$) inside the PDMS sheet. Figures 2(a)–2(c) demonstrate Blu-ray disk imaging using the developed superlensing objectives. In Fig. 2(a), the SEM image reveals that the disk consists of $200\ \text{nm}$ gratings separated $100\ \text{nm}$ away. Figures 2(b)–2(c) show the images obtained using an Olympus BX60 microscope equipped with the developed superlensing objective lenses with the following parameters: Fig. 2(b) with OB ($100\times$, NA0.90) + CMS ($67\ \mu\text{m}$ BaTiO_3 in PDMS) and Fig. 2(c) with OB ($100\times$, NA0.90) + CMS ($22\ \mu\text{m}$ BaTiO_3 in PDMS). As can be seen, both lenses can clearly resolve the $100\ \text{nm}$ features, which is beyond the classical diffraction limit of $300\ \text{nm}$. The smaller diameter BaTiO_3 superlens in Fig. 2(c) offers a larger magnification factor ($M \sim 6\times$) over the larger sized BaTiO_3 superlens ($M \sim 2\times$) in Fig. 2(b). This is caused by the shorter focal length of a smaller sized microsphere lens in the virtual imaging mode [12]. The central zone of the resulting image appears a bit overexposed in Fig. 2(b) due to the reflected beams by the Blu-ray substrate. This phenomenon is less obvious in smaller particles [Fig. 2(c)]. In microsphere superlens imaging, artificial images are always an issue and one should pay particular attention to it. The artificial images can be excluded by rotating the imaging samples.

Let's turn our eye to another sample, the adenoviruses sample. These virus particles are nearly spherical in shape with a diameter around $90\text{--}100\ \text{nm}$ [Fig. 2(d)]. They are

sub-diffraction-limited and are difficult to observe using conventional microscopes. Figure 2(e) shows a super-resolution image obtained using a superlensing objective lens formed by an $80\times$, NA0.90 objective and a $70\ \mu\text{m}$ BaTiO_3 microsphere. The viruses are aggregated in clusters in our sample, but it was possible to isolate them by zooming in on the image. The magnified particle size is about $200\ \text{nm}$ in Fig. 2(f), which means the real virus size is around $100\ \text{nm}$ since the $70\text{-}\mu\text{m}$ BaTiO_3 superlens offers a magnification factor around 2 in the experimental condition. Compared to Fig. 2(b), here the central zone doesn't have a bright spot due to reflection by the underlying substrate; this is because virus particles are deposited on a transparent glass slider that has much less reflection compared to a Blu-ray disk.

B. Scanning Imaging and Image Stitching

In our superlensing objective lens, the microsphere superlens is synchronized with an objective lens. During the scanning operation, both parts of the lens will move together simultaneously, and their relative position is kept constant. This is beneficial to scanning imaging since it ensures that the same particle lens is used in imaging. It is also possible to have multiple particle lenses in parallel for simultaneous scanning imaging. In our experiments, we evaluated scanning imaging of different samples, including the adenovirus samples. However, due to lens-sample contacting requirements, we had some difficulty in scanning imaging of virus samples, since the virus particles were dragged by the lens during scanning. This is due to the virus particles not being well fixed on the glass slides. This may not be the case for cell samples, which could be immobilized on glass slides, and is the plan of our next step experiments. In this study, scanning

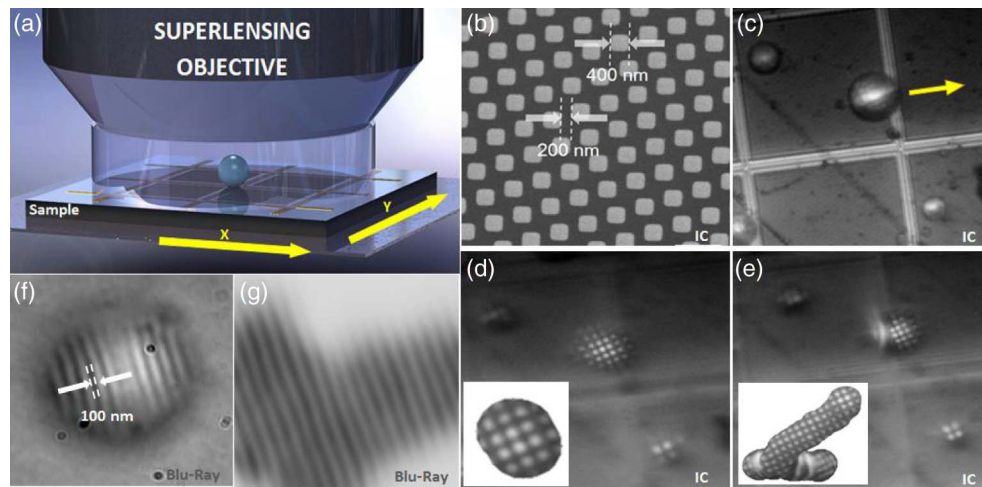


Fig. 3. Scanning super-resolution imaging and image stitch. (a) Scanning schematics. (b) Scanning direction of IC chip sample (c) SEM of IC chip. (d) IC scanning image position 1. (e) IC scanning position 2 (see Visualization 1 for the scanning movie). Insets show stitched image following scanning paths. (f) Blu-ray sample imaged by microsphere. (g) Stitched image of Blu-ray scanning.

imaging was performed with a well-structured semiconductor IC chip and Blu-ray disk sample to demonstrate the feasibility of scanning imaging using a developed superlensing objective lens, which was shown in Fig. 3. To reduce the friction between the lens and the sample, we evaluated different lubricant media, including DI water, IPA, silicone oil, and WD-40. WD-40 produces the best lubrication effect so it was used in the scanning experiments shown in Fig. 3. The IC chip in Fig. 3(b) has features of 200 nm and 400 nm, which are easy to observe using the new lens. The scanning process was video recorded (see Visualization 1). Comparing Figs. 3(c)–3(e), we can see the scanning takes place along the indicated scanning direction in Fig. 3(c), and high-resolution images were taken at different spatial positions. Stitching images produces a larger-sized picture covering scanned sample regions of interest following the scanning path [see demonstration in the insets of Figs. 3(d) and 3(e)]. The image stitching code based on MATLAB language that was developed in-house works automatically for a sequence of frames with moderate movement between the adjacent frames. The location and size of a superlens imaging region in the first image frame are specified. In the subsequent frames, the location can change gradually. To compensate for this, with the assumption that superlens imaging regions are in focus and thus contain more image features, the algorithm searches in the neighborhood of the location from the previous frame to find the region with most significant total edge strengths. For each extracted region, radial distortion correction is applied. The correction parameter is estimated based on images with a regular grid structure (e.g., an image on the IC chip). From the first extracted region, the images are stitched sequentially, and the optimal offset between adjacent extracted regions is calculated based on maximizing the normalized cross correlation. This criterion works more effectively than e.g., the sum of squared differences because it copes better with a variation in image brightness. The stitched images are obtained by integrating pixels from all the extracted regions with corresponding offsets applied. To avoid visible boundaries between regions from different

frames, alpha blending is used so for the stitched image pixels where multiple source regions overlap, a combination of their contributions is used. Similar scanning experiments also were performed with a Blu-ray disk sample [Fig. 3(f)], where the stitched image was shown in Fig. 3(g).

4. MECHANISM AND DISCUSSION

Light interaction with spherical particles can be simulated using the classical Mie theory. Figure 4 shows examples of calculated electric field intensity $|E|^2$ distribution across a cross-sectional plane of an 18 μm and a 67 μm BaTiO₃ microsphere ($n = 1.90$) embedded in PDMS ($n = 1.40$) under different illumination wavelengths, covering the 400 nm to 700 nm spectrum range of a typical white lighting source. The corresponding size parameter for each case, defined as $q = \pi D/\lambda$, where D is the particle diameter and λ the wavelength, was also indicated in the figure. A video was provided (see Visualization 2) that offers a systematic view of the evolution of field distribution for size parameters $0.1 \leq q \leq 628$, with a step accuracy of $\Delta q = 0.1$. From Fig. 4 we can see, in addition to the well-known photonic nanojet-focusing modes by microspheres [Figs. 4(a), 4(c), 4(d), and 4(f)], strong internal focusing modes featuring hugely enhanced intensity peaks inside the particle could be excited at particular wavelengths [Figs. 4(b) and 4(e)]. All these modes will play a role in super-resolution image formation.

The imaging sample in contact with microsphere is illuminated by the microsphere lens; super-resolution arises from the strong near-field interaction between the microsphere lens and the underlying nano-objects, which leads to the conversion of surface-bounded high spatial frequency evanescent waves into propagating waves [14,32]. Such an interaction process is quite complex and is out of the scope of Mie theory. An example calculation for the coupled microsphere-substrate system was demonstrated in a previous publication [14] using a full-wave simulation approach. It was noted that such a conversion process is sensitive to the substrate properties and the gap distance

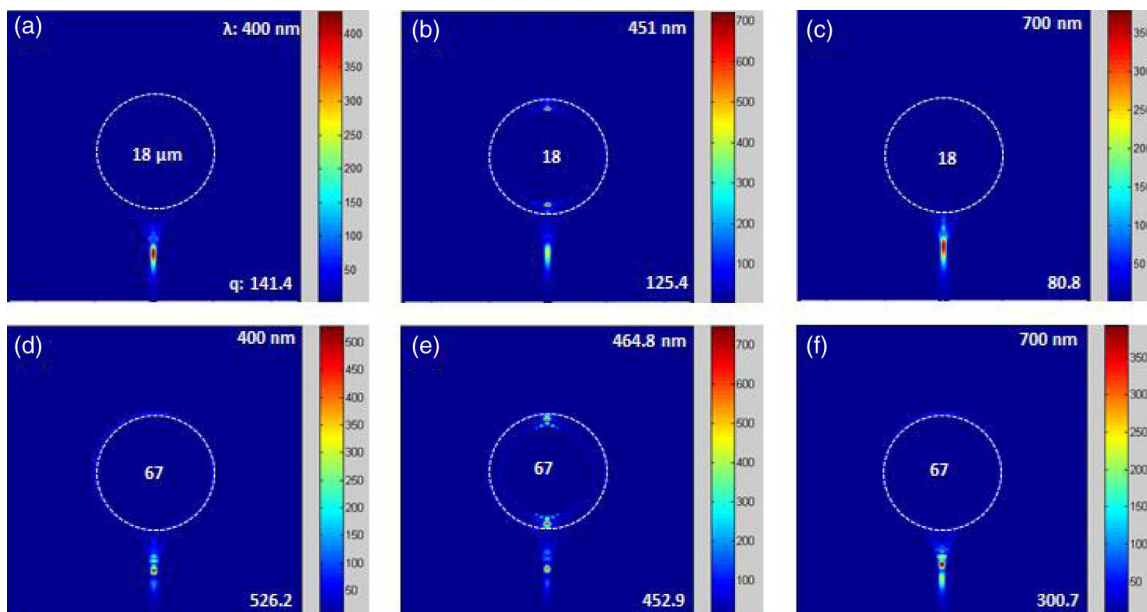


Fig. 4. Electric field intensity ($|E|^2$) distribution in the cross sectional plane of 18 μm and 67 μm diameter BaTiO₃ microsphere embedded in PDMS material illuminated by different visible wavelengths. The light is incident from top to bottom, with electric field polarized from left to right. q is the size parameter defined as $q = \pi D/\lambda$, where D is the particle diameter and λ the wavelength; see Visualization 2 for the animation of field evolution as a function of size parameter q .

between lens and object. The technique requires a gap distance below the wavelength scale and, ideally, a zero distance gap is desired [14]. Besides the substrate effect, other factors such as different NA illumination, the incident illumination angle, and the microscope image plane have been found to also influence the experimental resolution and magnification. These uncertainties are challenges, but also opportunities, for next-generation dielectric superlens development. For example, inspired by enhancing the lens and sample evanescent coupling for a better super-resolution, we recently used a high-index TiO₂ nanoparticle as a building block to form a mouldable micro-sized lens that was deposited on an imaging sample, leading to perfect contacting with an imaging sample and meanwhile supporting extremely high evanescent-to-propagation conversion efficiency. This new superlens design has shown greatly improved imaging contrast and field of view over all previously reported designs, and has a record white light super-resolution of 45 nm [25].

Besides the constant contacting scanning mode, we are currently developing a new “tapping scanning” imaging mode to minimize the friction issues during contacting imaging. Our work reported here laid down a solid foundation for further development of superlensing objective lens technology and we believe it is the first kind of such lens in the literature. We expect the key problem of contacting scanning will be circumvented in future designs, and a contactless superlensing objective lens will be developed. This may be achieved by combining optical superoscillatory mask design with existing superlensing objective design.

5. CONCLUSION

To summarize, we have demonstrated a new type of microscope objective lens, a superlensing objective lens that integrates a conventional objective lens and a coverslip-like microsphere

superlens. The new lens has advantages in usability and is able to image the sample with super-resolution in both static and scanning modes. A resolution of 100 nm under white light illumination has been demonstrated. The developed superlensing objective lens has potential to be further developed into a commercial product that would transform an existing microscope into a nanoscope.

Funding. Welsh Crucible; Bangor University (006311); Cardiff University (510435); Sêr Cymru National Research Networking Advanced Engineering and Materials (NRN113, NRNF66).

REFERENCES

1. E. Abbe, “Beitrage zur Theorie des Mikroskops und der mikroskopischen Wahrnehmung,” *Archiv Mikroskop. Anat.* **9**, 413–420 (1873).
2. X. Zhang and Z. W. Liu, “Superlenses to overcome the diffraction limit,” *Nat. Mater.* **7**, 435–441 (2008).
3. D. W. Pohl, W. Denk, and W. Lanz, “Optical stethoscopy: image recording with resolution $\lambda/20$,” *Appl. Phys. Lett.* **44**, 651–653 (1984).
4. J. B. Pendry, “Negative refraction makes a perfect lens,” *Phys. Rev. Lett.* **85**, 3966–3969 (2000).
5. E. T. Rogers, J. Lindberg, T. Roy, S. Savo, J. E. Chad, M. R. Dennis, and N. I. Zheludev, “A super-oscillatory lens optical microscope for subwavelength imaging,” *Nat. Mater.* **11**, 432–435 (2012).
6. M. Davy, J. G. Minonzio, J. de Rosny, C. Prada, and M. Fink, “Influence of noise on subwavelength imaging of two close scatterers using time reversal method: theory and experiments,” *Prog. Electromagn. Res.* **98**, 333–358 (2009).
7. V. Smolyaninova, C. Jensen, W. Zimmerman, A. Johnson, D. Schaefer, and I. Smolyaninov, “Lithographically fabricated magnifying Maxwell fisheye lenses,” *Photonics* **3**, 8 (2016).
8. J. H. Park, C. Park, Y. H. Cho, and Y. Park, “Scattering super-lens: subwavelength light focusing and imaging via wavefront shaping in

- complex media," in *Conference on Lasers and Electro-Optics (CLEO)* (2014).
9. S. W. Hell and J. Wichmann, "Breaking the diffraction resolution limit by stimulated emission: stimulated-emission-depletion fluorescence microscopy," *Opt. Lett.* **19**, 780–782 (1994).
 10. E. Betzig, G. H. Patterson, R. Sougrat, O. W. Lindwasser, S. Olenych, J. S. Bonifacino, M. W. Davidson, J. Lippincott-Schwartz, and H. F. Hess, "Imaging intracellular fluorescent proteins at nanometer resolution," *Science* **313**, 1642–1645 (2006).
 11. S. T. Hess, T. P. K. Girirajan, and M. D. Mason, "Ultra-high resolution imaging by fluorescence photoactivation localization microscopy," *Biophys. J.* **91**, 4258–4272 (2006).
 12. Z. Wang, W. Guo, L. Li, B. Luk'yanchuk, A. Khan, Z. Liu, Z. Chen, and M. Hong, "Optical virtual imaging at 50 nm lateral resolution with a white-light nanoscope," *Nat. Commun.* **2**, 218 (2011).
 13. Z. B. Wang and L. Li, "White-light microscopy could exceed 50 nm resolution," *Laser Focus World* **47**, 61–64 (2011).
 14. Z. B. Wang, "Microsphere super-resolution imaging," in *Nanoscience*, J. T. Paul and O. Brien, eds. (Royal Society of Chemistry, 2016), pp. 193–210.
 15. Z. G. Chen, A. Taflove, and V. Backman, "Photonic nanojet enhancement of backscattering of light by nanoparticles: a potential novel visible-light ultramicroscopy technique," *Opt. Express* **12**, 1214–1220 (2004).
 16. Y. F. Lu, L. Zhang, W. D. Song, Y. W. Zheng, and B. S. Luk'yanchuk, "Laser writing of a subwavelength structure on silicon (100) surfaces with particle-enhanced optical irradiation," *J. Exp. Theor. Phys. Lett.* **72**, 457–459 (2000).
 17. Y. Yan, L. Li, C. Feng, W. Guo, S. Lee, and M. H. Hong, "Microsphere-coupled scanning laser confocal nanoscope for sub-diffraction-limited imaging at 25 nm lateral resolution in the visible spectrum," *ACS Nano* **8**, 1809–1816 (2014).
 18. A. Darafsheh, N. I. Limberopoulos, J. S. Derov, D. E. Walker, and V. N. Astratov, "Advantages of microsphere-assisted super-resolution imaging technique over solid immersion lens and confocal microscopes," *Appl. Phys. Lett.* **104**, 061117 (2014).
 19. A. Darafsheh, G. F. Walsh, L. Dal Negro, and V. N. Astratov, "Optical super-resolution by high-index liquid-immersed microspheres," *Appl. Phys. Lett.* **101**, 141128 (2012).
 20. A. Darafsheh, G. Wu, S. Yang, and J. C. Finlay, "Super-resolution optical microscopy by using dielectric microwires," in *Three-Dimensional and Multidimensional Microscopy: Image Acquisition and Processing XXIII* (SPIE, 2016), paper 97130U.
 21. G. Q. Gu, R. Zhou, H. Y. Xu, G. X. Cai, and Z. P. Cai, "Subsurface nano-imaging with self-assembled spherical cap optical nanoscopy," *Opt. Express* **24**, 4937–4948 (2016).
 22. R. Ye, Y. H. Ye, H. F. Ma, J. Ma, B. Wang, J. Yao, S. Liu, L. L. Cao, H. H. Xu, and J. Y. Zhang, "Experimental far-field imaging properties of ~5- μm diameter spherical lens," *Opt. Lett.* **38**, 1829–1831 (2013).
 23. B. Yan, L. Y. Yue, and Z. B. Wang, "Engineering near-field focusing of a microsphere lens with pupil masks," *Opt. Commun.* **370**, 140–144 (2016).
 24. L. Y. Yue, B. Yan, and Z. B. Wang, "Photonic nanojet of cylindrical metalens assembled by hexagonally arranged nanofibers for breaking the diffraction limit," *Opt. Lett.* **41**, 1336–1339 (2016).
 25. W. Fan, B. Yan, Z. B. Wang, and L. M. Wu, "Three-dimensional all-dielectric metamaterial solid immersion lens for subwavelength imaging at visible frequencies," *Sci. Adv.* **2**, e1600901 (2016).
 26. J. N. Monks, B. Yan, N. Hawkins, F. Vollrath, and Z. B. Wang, "Spider silk: mother nature's bio-superlens," *Nano Lett.* **16**, 5842–5845 (2016).
 27. L. A. Krivitsky, J. J. Wang, Z. B. Wang, and B. Luk'yanchuk, "Locomotion of microspheres for super-resolution imaging," *Sci. Rep.* **3**, 3501 (2013).
 28. J. X. Li, W. J. Liu, T. L. Li, I. Rozen, J. Zhao, B. Bahari, B. Kante, and J. Wang, "Swimming microrobot optical nanoscopy," *Nano Lett.* **16**, 6604–6609 (2016).
 29. Z. Wang, "Improvements in and relating to lenses," PCT patent PCT/GB2014/052578 (26 February 2015).
 30. K. W. Allen, N. Farahi, Y. Li, N. I. Limberopoulos, D. E. Walker, A. M. Urbas, V. Liberman, and V. N. Astratov, "Super-resolution microscopy by movable thin-films with embedded microspheres: resolution analysis," *Ann. Phys.* **527**, 513–522 (2015).
 31. V. N. Astratov and A. Darafsheh, "Methods and systems for super-resolution optical imaging using high-index of refraction microspheres and micro-cylinders," U.S. patent 20140355108 A1 (4 Dec. 2014).
 32. X. Hao, C. Kuang, Z. Gu, Y. Wang, S. Li, Y. Ku, Y. Li, J. Ge, and X. Liu, "From microscopy to nanoscopy via visible light," *Light Sci. Appl.* **2**, e108 (2013).